photonics

MDPI

Article

Impact of LD Spectra on Efficiency of Yb-Doped Fiber Laser

Fengyun Li [1], Yi Shi [1], Chun Zhang [1], Qiuhui Chu [1], Lingli Huang [1,2], Haoyu Zhang [1], Qiang Shu [1], Yu Wen [1], Xingchen Jiang [1,2], Zixiang Gao [1,2], Honghuan Lin [1] and Rumao Tao [1,*]

[1] Laser Fusion Research Center, China Academy of Engineering Physics, Mianyang 621900, China; lify@pku.edu.cn (F.L.); shiyi1616@163.com (Y.S.); wsrf@mail.ustc.edu.cn (C.Z.); chuqiuhui809@caep.cn (Q.C.); linglihuang@njust.edu.cn (L.H.); hao_yu_zhang@126.com (H.Z.); shuqiang2018@caep.cn (Q.S.); wenyu22@gscaep.ac.cn (Y.W.); jxc980124@njust.edu.cn (X.J.); g18727973510@163.com (Z.G.); happylin2003@yeah.net (H.L.)

[2] School of Electronic and Optical Engineering, Nanjing University of Science and Technology, Nanjing 210094, China

* Correspondence: supertaozi@163.com

Abstract

The spectral characteristics of pump laser diodes (LDs) introduce significant ambiguity into the performance evaluation of high-power ytterbium-doped fiber lasers (YDFLs), obscuring their intrinsic efficiency and hindering reliable system design. Here, we introduce a rigorous quantitative framework that decouples these pump-induced effects by referencing laser performance to the absorbed, rather than the launched, pump power. Our analysis demonstrates that the widely reported discrepancies in conventional optical-to-optical (OO) and slope efficiencies are governed almost entirely by variations in pump absorption, while the influence of the quantum defect is negligible. This approach provides a robust metric for intrinsic laser performance that is independent of the LD's spectral properties, proving particularly valuable for systems pumped by non-wavelength-stabilized LDs (nWS-LDs). We uncover a non-monotonic evolution of the unabsorbed residual pump power, revealing that the peak thermal load on system components occurs at an intermediate operational state, not at maximum pump power. This finding challenges conventional thermal management strategies and is critical for ensuring the long-term operational reliability of high-power YDFLs.

Keywords: high-power fiber laser; laser diode spectrum; optical-to-optical conversion efficiency; pump absorption; slope efficiency; thermal management

Received: 9 July 2025
Revised: 31 July 2025
Accepted: 9 August 2025
Published: 11 August 2025

Citation: Li, F.; Shi, Y.; Zhang, C.; Chu, Q.; Huang, L.; Zhang, H.; Shu, Q.; Wen, Y.; Jiang, X.; Gao, Z.; et al. Impact of LD Spectra on Efficiency of Yb-Doped Fiber Laser. *Photonics* **2025**, *12*, 806. https://doi.org/10.3390/photonics12080806

1. Introduction

Over the past several decades, extensive research has been devoted to YDFLs in the high-power scaling regime for widespread applications in material processing and military technology due to a confluence of advantages including extraordinary beam quality, efficient thermal management, mechanical robustness, and high conversion efficiency [1–7]. The rapid growth of YDFLs has been considerably pushed by amazing advancements in LDs, which are exploited as high-efficiency pump sources [4]. LD modules can now produce multi-kilowatts of output power with electric–optical efficiency over 52% [8] and brightness of up to 74 MW/(cm^2·str) [9], thanks to enhanced heat control and numerous combining techniques. Figure 1a shows a prominent and narrow spear-like absorption cross-section peak in ytterbium-doped fiber (YDF) near 976 nm, indicating high sensitivity to variations in the pump wavelength emitted by LDs [10,11].

Considerable waste heat generated at the diode junction arising from non-radiative transition or quantum defects increases the junction temperature during operation, resulting in a spectral redistribution of the emitting light and a central wavelength drift from 0.14 to 0.32 nm/K [12–14], which may deviate far from the YDF absorption peak. To achieve a consistent expected absorption proportion, variations in LD-emitting spectra consequently result in changes in absorbtion rate and matching YDF length, which further have a significant influence on laser properties. Numerous studies have been devoted to studying the associated effects, including wide temperature operation [10,15], stimulated Raman scattering (SRS) suppression [16–18], stimulated Brillouin scattering (SBS) suppression [19], and transverse mode instability (TMI) mitigation [13,20–25]. In 2016, Huang et al. introduced the absorption degradation ratio factor (ADR) as a guide reference for pump selection and experimentally compared the OO efficiency between wavelength-stabilized (WS-LD) and nWS-LD [26], demonstrating the spectral influences on laser efficiencies and performances. Similar phenomena were observed, especially for nWS-LD pumped systems, when the laser operates with varied LD-emitting spectra [14,25,27–30]. However, the major influence of LD spectral characteristics on efficiency is still poorly measured, preventing a more thorough exploration of the underlying mechanisms determining their relationship. Furthermore, a better understanding of this relationship is critical for managing the longitudinal pump absorption profile by precisely adjusting the LDs' output spectra. This control helps balance the opposing requirements for pump absorption between nonlinear effects (SRS or SBS) and TMI, allowing for increased power scaling in near-diffraction-limit laser systems [17,19,31–33].

This work provides a quantitative assessment of the effect of different LD spectrum emission characteristics on OO efficiency. To ensure a systematic evaluation and mitigate the effects of inherent device-to-device differences, our methodology combines each LD's observed emission spectrum and, more importantly, bases the computation of the OO efficiency on the absorbed pump power rather than the launched one. This enhanced approach not only provides consistency in the measured OO efficiencies but also allows for the correction of differences in the calculated slope efficiencies.

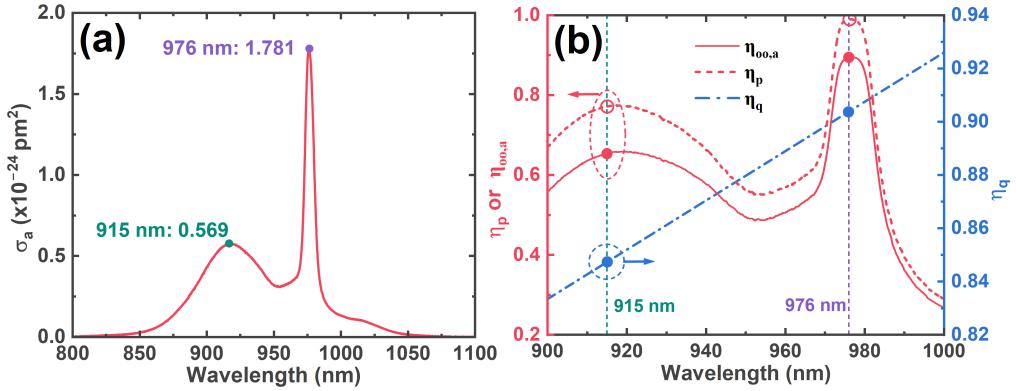

Figure 1. (**a**) Absorption cross-section of YDF. (**b**) $\eta_{oo,a}$, η_p, η_q versus pumping wavelength λ under a $\delta(\lambda)$ assumption for $S(I, \lambda)$.

2. Theoretical Analysis

The OO efficiency, defined as the ratio of the output laser power P_o to the pump power P_p, is a fundamental metric for evaluating energy conversion performance across a broad spectrum of laser systems [34–39]. The pump power can be defined as either the total launched power $P_{p,l}$ or the power absorbed by the gain medium $P_{p,a}$. This results in two separate efficiency metrics: $\eta_{oo,l} = P_o/P_{p,l}$, which measures overall system

efficiency, and $\eta_{oo,a} = P_o / P_{p,a}$, which characterizes the intrinsic laser conversion process and is independent of pump absorption characteristics. This distinction also extends to the slope efficiency, which quantifies the differential conversion performance and is usually calculated from a linear fit of P_o versus P_p. As a result, two types of slope efficiency are defined: $\eta_{sl,l} = \mathrm{d}P_o / \mathrm{d}P_{p,l}$ and $\eta_{sl,a} = \mathrm{d}P_o / \mathrm{d}P_{p,a}$, which correspond to the two kinds of pump power metrics. In high-power YDFLs, efficiencies $\eta_{oo,l}$ and $\eta_{sl,l}$ based on the launched pump power are primarily reported because of their relative simplicity of measurement.

The absorption of pump light in an optically pumped YDFL is fundamentally governed by the Beer–Lambert law [40]. In a YDF with a uniform core, the absorption coefficient at a specific pump wavelength λ is given by [41,42]

$$\alpha(\lambda) = \sigma(\lambda) n \Gamma \tag{1}$$

where $\sigma(\lambda)$ represents the absorption cross-section of Yb ions at wavelength λ, as illustrated in Figure 1a, while n and Γ represent the Yb doping concentration and pump overlap factor, respectively. The Beer–Lambert rule states that pump power diminishes exponentially as fiber length L increases [43]. To account for the whole emission spectrum of an LD running at a current I, the residual pump power $P_{p,r}(I)$ is derived by integrating the contributions from all spectral components:

$$P_{p,r}(I) = \int_0^\infty P_{p,l}(I,\lambda) \mathrm{e}^{-\alpha(\lambda)L} \, \mathrm{d}\lambda = P_{p,l}(I) \int_0^\infty S(I,\lambda) \mathrm{e}^{-\sigma(\lambda) n \Gamma L} \, \mathrm{d}\lambda \tag{2}$$

Here, $P_{p,l}(I)$ represents the total launched pump power and $S(I,\lambda)$ represents the normalized power spectral density of the LD emission at current I. The absorbed pump power $P_{p,a}$ is the complement to the residual power $P_{p,r}$. The pump absorption efficiency η_p can be obtained as follows:

$$\eta_p(I) = \frac{P_{p,a}(I)}{P_{p,l}(I)} = 1 - \frac{P_{p,r}(I)}{P_{p,l}(I)} = 1 - \int_0^\infty S(I,\lambda) \mathrm{e}^{-\sigma(\lambda) n \Gamma L} \, \mathrm{d}\lambda \tag{3}$$

The current-dependent factor $\eta_p(I)$ mediates the relationship between launched power-based OO efficiency $\eta_{oo,l}$ and absorbed power-based efficiency $\eta_{oo,a}$. To better understand the conversion process, $\eta_{oo,a}$ can be separated into two components, quantum conversion efficiency $\eta_q(I)$, which is dependent on the LD spectrum, and intrinsic efficiency η_i, which is generally considered to arise from factors such as background loss of fiber or cavity, splicing loss and inadequate reflectivity of fiber Bragg grating (FBG), immune to variations in LDs' output power or spectra. This leads to the following expression:

$$\eta_{oo,l}(I) = \frac{P_o(I)}{P_{p,l}(I)} = \frac{P_o(I)}{P_{p,a}(I)/\eta_p(I)} = \eta_p(I) \cdot \eta_{oo,a}(I) = \eta_p(I) \cdot \eta_q(I) \cdot \eta_i \tag{4}$$

The quantum conversion efficiency is governed by the energy loss from quantum defects, which occurs from the wavelength shift $hc(1/\lambda - 1/\lambda_s)$ between the pump wavelength λ and the signal wavelength λ_s fixed at 1080 nm. Integrating over the full pump spectrum yields the total quantum conversion efficiency for a particular spectral distribution $S(I,\lambda)$ as follows:

$$\eta_q(I) = \int_0^\infty S(I,\lambda) \lambda / \lambda_s \, \mathrm{d}\lambda \tag{5}$$

To demonstrate the wavelength-dependent character of these efficiencies, we investigate a monochromatic pump source by setting the spectrum to a delta function, $S(\lambda) = \delta(\lambda)$, between 900 and 1000 nm. The resulting efficiency variations, calculated using Equations (1)–(5), are presented in Figure 1b. As seen in the figure, the efficiencies at

976 nm and 915 nm exhibit a significant disparity, emphasizing the importance of pump wavelength. The powers, efficiencies, and their relationships are illustrated by the flowchart in Figure 2.

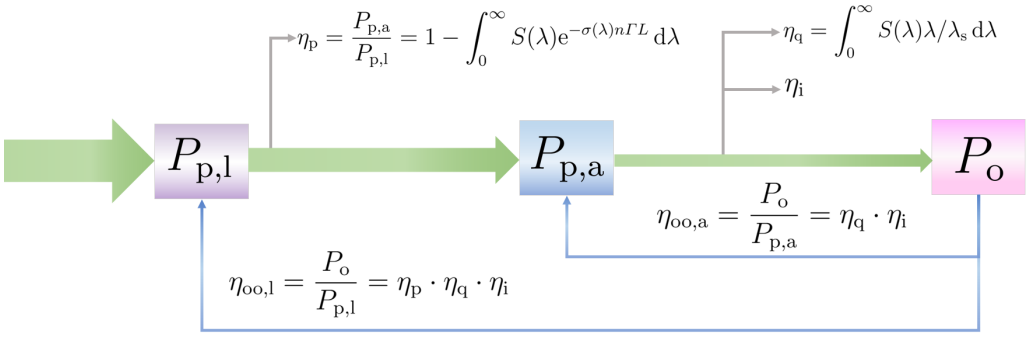

Figure 2. Illustration of laser OO conversion efficiency η_{oo} decomposition.

3. Experimental Setup

To investigate the influence of LD spectral characteristics on conversion efficiency, we built a YDFL oscillator as shown in Figure 3. While this study utilized an oscillator architecture for simplicity, the underlying physical principles are broadly applicable to different YDFL systems. The system was based on a counter-pumped resonant cavity formed by an 8 m YDF with core/cladding diameter 14/250 µm and NA 0.07/0.46, placed between a high-reflectivity FBG (HR FBG) with reflectance value greater than 99.9% and full width at half maximum (FWHM) around 3 nm and an output coupling FBG (OC FBG) with a reflectance value ~10% and FWHM around 1 nm, both centered around 1080 nm. The YDF length was optimized to ensure acceptable total 20 dB pump absorption, with a measured absorption coefficient of 2.6 dB/m at 976 nm. The fiber was coiled with a diameter of about 80 mm on a water-cooled plate maintained at 22 °C to promote almost-single-mode operation and thermal stability.

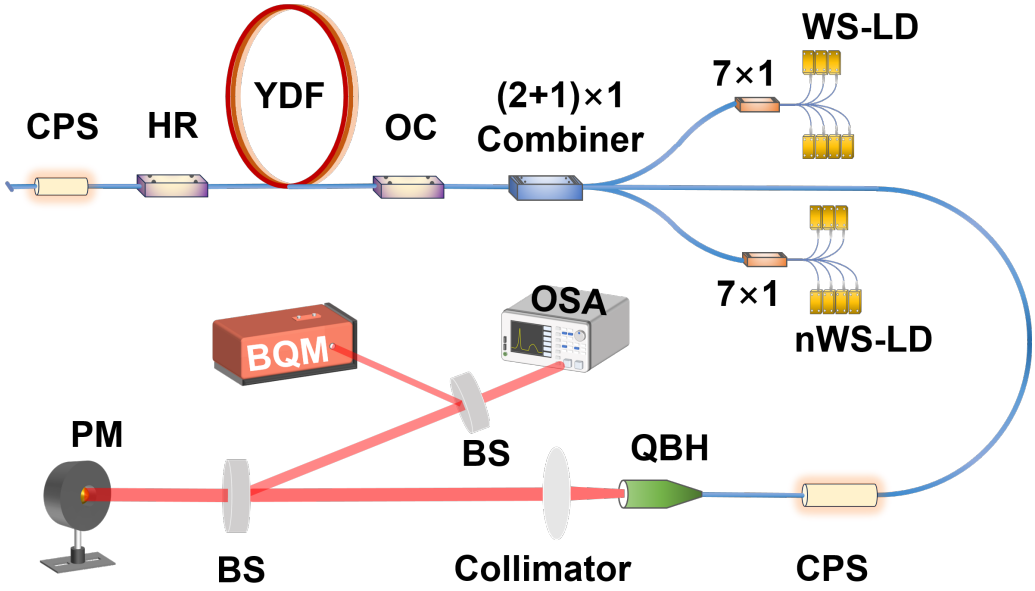

Figure 3. Schematic diagram of counter-pumped fiber oscillator and corresponding measuring system.

The pump source consisted of two distinct LD groups. The first group consisted of seven WS-LD modules, each capable of delivering up to 90 W of power around a target wavelength of 976 nm. These modules were connected via a 7 × 1 pump combiner and

injected into the cavity via one pump port of a (2 + 1) × 1 pump and signal combiner (PSC). Another group of nWS-LD modules was similarly constructed and injected via the PSC's other pump port. The 14/250 μm signal pigtails of the PSC matched the YDF and the 220/242 μm pump pigtails matched the output of the 7 × 1 combiner. A cladding power stripper (CPS) was installed after the OC FBG to remove any residual cladding light before the laser was terminated with a quartz-block-head (QBH) for free space output. Another CPS was fused to the HR FBG pigtail to filter unabsorbed pump light, with its end face angle cleaved at 8° to prevent Fresnel reflection. All passive fibers, including those in the CPS and QBH, were germanium-doped fibers (GDFs) with core/cladding diameters of 14/250 μm.

The QBH output laser beam was collimated and steered through a high-transmission beam splitter (BS) with a reflectivity of 4%. A power meter (PM) captured the main transmission beam and measured the output power. A second 4% BS sampled the reflected portion and sent the light to a BQM system for spatial characterization and an OSA for spectral analysis. To isolate the influence of the pump source, the oscillator was operated under similar conditions, with the only difference being the active LD group (WS-LD or nWS-LD). This design enabled any observed differences in laser performance to be directly linked to the spectral properties of the different LDs.

Figure 4 illustrates the emission spectra of the WS-LD and nWS-LD groups at driver currents ranging from 1 A to 11 A. In the nWS-LD group, increasing the current caused a significant red-shift [44] in the central wavelength, from 968.73 nm to 977.35 nm, as well as a spectral broadening of the FWHM from 0.94 nm to 3.84 nm due to thermal heating-induced refractive index change, hole burning, and gain saturation [45,46]. The FWHM at lower currents was slightly underestimated due to the spectrum's multi-peak. In stark contrast, the WS-LD group demonstrated outstanding spectral stability. The central wavelength remained tightly locked at a mean value of 976.14 nm, with a standard deviation of only 0.07 nm across the full current range. Similarly, the FWHM was confined to a small band with an average of 0.21 nm and a standard deviation of 0.02 nm. As seen in Figure 4b, the stabilizing effect in WS-LDs became more evident at higher currents as more optical power was focused near the 976 nm locking wavelength. A detailed summary of the central wavelengths and FWHMs for both LD groups is provided in Table 1.

Table 1. LD output power and spectral parameters for nWS- and WS-LD under different currents.

Current/A	nWS-LD			WS-LD		
	Power/W	**λ_c/nm**	**FWHM/nm**	**Power/W**	**λ_c/nm**	**FWHM/nm**
1	84	968.73	0.94	82	976.03	0.18
2	142	968.81	1.86	138	976.05	0.18
3	201	968.79	3.01	205	976.07	0.19
4	259	971.31	3.07	258	976.09	0.20
5	320	971.96	2.80	321	976.12	0.21
6	374	971.99	3.09	376	976.15	0.21
7	434	972.47	3.48	436	976.18	0.21
8	488	974.16	4.19	494	976.20	0.23
9	538	974.74	4.54	550	976.17	0.21
10	581	976.19	4.11	601	976.23	0.25
11	618	977.35	3.84	627	976.22	0.24
Mean	–	972.41	3.18	–	976.14	0.21
Std.	–	2.97	1.06	–	0.07	0.02

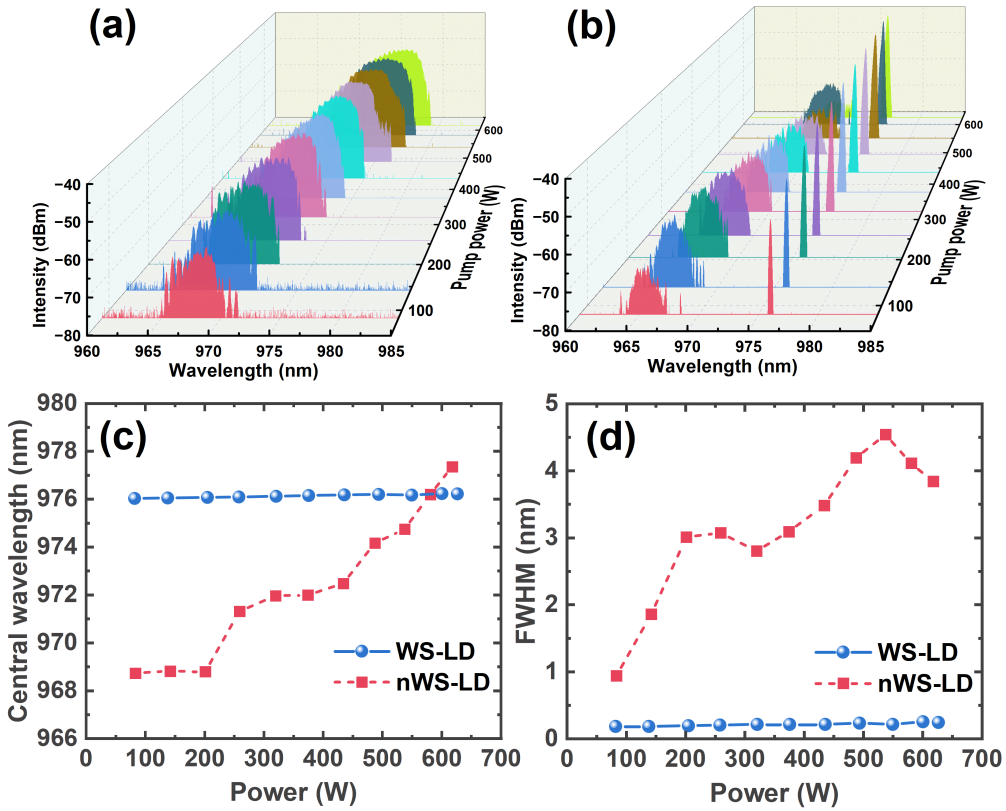

Figure 4. Output spectra of (**a**) nWS- and (**b**) WS-LD modules. (**c**) Central wavelength (λ_c) and (**d**) FWHM of nWS- and WS- modules under different operating powers.

4. Results and Discussion

Figure 5a shows the output power P_o as a function of launched pump power $P_{p,l}$ for both WS- and nWS-LD pumping schemes. In all cases, P_o increased roughly linearly with $P_{p,l}$, reaching a maximum of about 400 W when the pump power exceeded 600 W. Figure 5b displays the OO efficiency $\eta_{oo,l}$ determined in relation to the launched power. When pumped by the WS-LD group, the oscillator consistently exhibited a greater $\eta_{oo,l}$ than the nWS-LD case. Their efficiency difference $\Delta\eta_{oo,l}$ was most noticeable at lower pump powers and steadily declined as the power increased, as shown in Figure 6d. This improved performance can be attributed to the superior spectral characteristics of the WS-LDs, which concentrated pump power on the 976 nm absorption peak of the YDF, resulting in more efficient energy conversion. A detailed analysis of the corresponding slope efficiency difference is provided in this section.

Despite variances in pump spectra and conversion efficiency, the output laser properties were fairly constant across the two pumping groups. The presence of multiple longitudinal modes in the oscillator cavity broadened the output laser spectrum to a linewidth of approximately 3.64 nm at maximum power, driven by nonlinear effects such as self-phase modulation, cross-phase modulation, and four-wave mixing [47]. Corresponding output spectra are shown in Figure 5c. The 14/250 μm YDF was a few-mode fiber that mainly supported the LP_{01} and LP_{11} modes. However, the YDF's tight coiling efficiently suppressed the higher-order mode (HOM), resulting in almost-single-mode operation. As a result, the output beam profile remained stable in Gaussian shape under both pumping conditions. At maximum output power, the beam quality factor M^2 was measured to be 1.216 and 1.235 in the x and y directions, respectively, confirming excellent beam quality, as shown in Figure 5d. The single-mode operation eliminated absorption influence from different mode distributions.

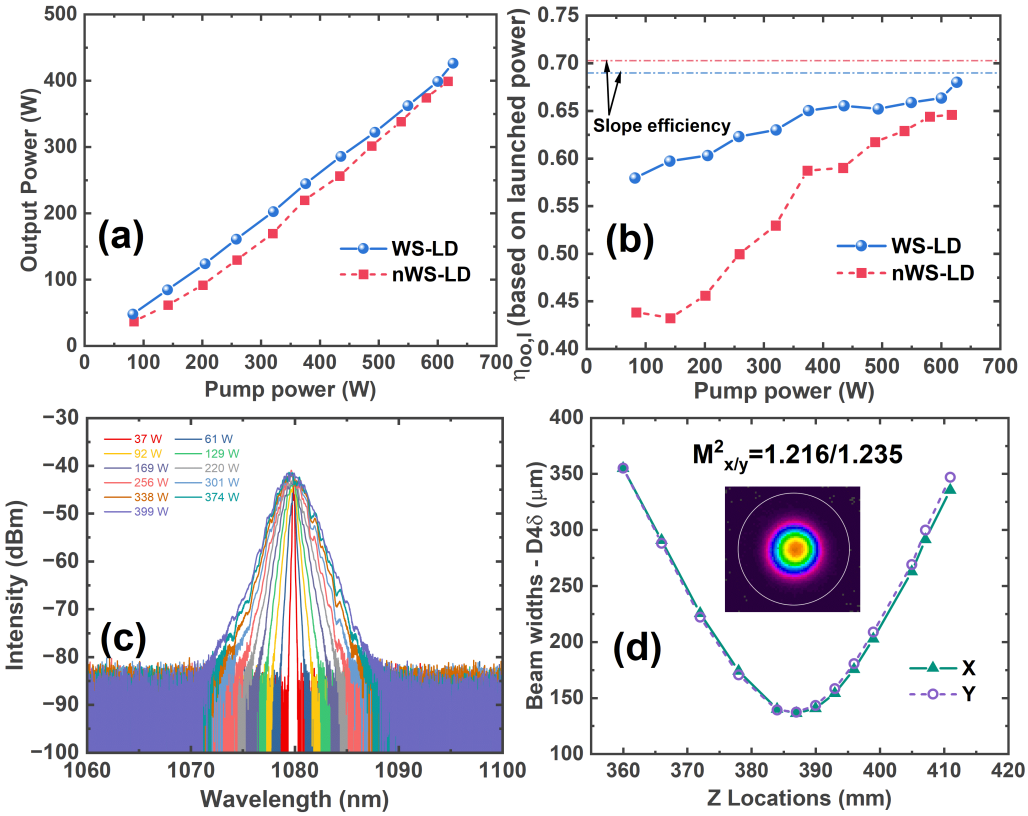

Figure 5. (**a**) Output power and (**b**) OO efficiency $\eta_{oo,l}$ under different WS- and nWS-LD pumping powers. (**c**) Optical spectra at different powers and (**d**) M^2 measurement at 399 W under nWS-LD pumping.

To quantify the roots of the observed efficiency discrepancy, we calculated the pump absorption efficiency η_p and the quantum efficiency η_q as functions of the launched pump power. To conduct these calculations, Equations (3) and (5) were numerically integrated with the measured LD spectra. The results for both WS- and nWS-LD configurations are presented in Figure 6a,b.

This research demonstrated that the pump absorption efficiency η_p was the primary cause of the difference in the OO efficiency $\eta_{oo,l}$. As shown in Figure 6a, η_p the WS-LD configuration maintained almost above 85% across all power levels, but nWS-LD started at a low of roughly 65% and gradually increased with power. This difference, which was most noticeable at low power levels, occurred because the nWS-LD spectrum was initially far from the 976 nm absorption peak. As the nWS-LD power grew, the spectrum shifted closer to 976 nm, causing its η_p to approach the WS-LD and converge toward unity. In contrast, Figure 6b shows that the quantum efficiency η_q exhibited relatively slight fluctuations, on the order of a few thousandths, for both LD types and across the entire operational range. This suggests that quantum defect variations had a minor impact on the overall efficiency difference.

Normalizing the output power to the absorbed pump power $P_{p,a}$ removed the dominant influence of η_p and revealed the absorbed power-based OO efficiency $\eta_{oo,a}$. As depicted in Figure 6c, the calculated $\eta_{oo,a}$ values for both the WS-LD and nWS-LD configurations were remarkably consistent, exhibiting nearly identical performance once the pump absorption effects were separated. This consistency was also reflected in the intrinsic efficiency η_i derived using Equation (4) and illustrated in Figure 6d, which closely tracked $\eta_{oo,a}$. A direct comparison of the efficiency differences $\Delta\eta_{oo,l}$, $\Delta\eta_{oo,a}$, and $\Delta\eta_i$ in Figure 6e

clearly reveals that the substantial changes in $\eta_{oo,l}$ were almost completely attributable to variations in η_p.

We show that the considerable variations in the generally reported OO efficiency $\eta_{oo,l}$ are principally driven by changes in pump absorption efficiency, which are generated by the spectral characteristics of the pump LDs. Efficiency based on absorbed power ($\eta_{oo,a}$ or η_i) provides a more precise and robust esitmate of the laser's intrinsic conversion capabilities while independent of the specific pump configuration.

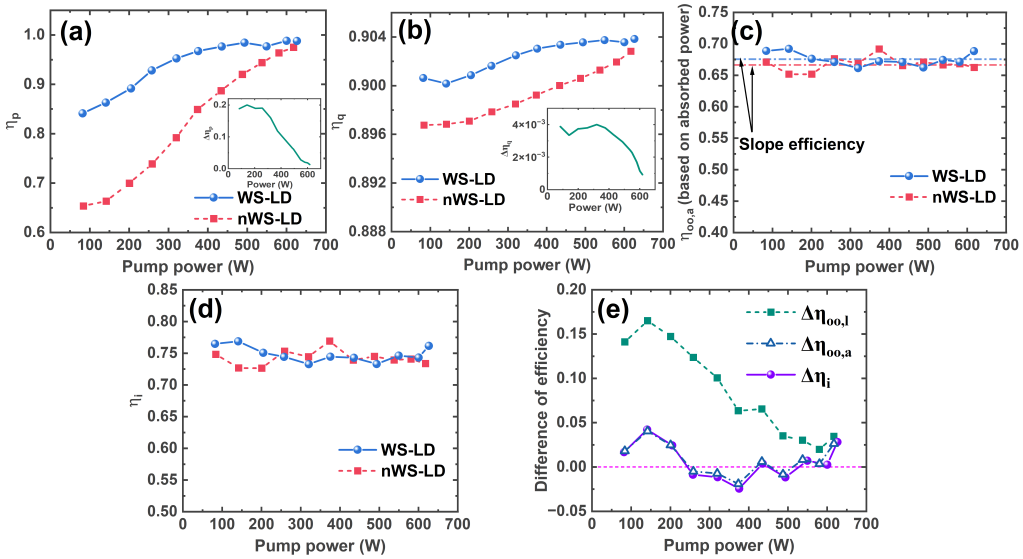

Figure 6. (**a**) Pump absorption efficiency η_p, (**b**) quantum conversion efficiency η_q, (**c**) OO efficiency $\eta_{oo,a}$, and (**d**) intrinsic efficiency η_i under different nWS- and WS-LD pumping powers. The inserts in (**a**,**b**) are corresponding differences between nWS- and WS-LD. (**e**) Conversion efficiency differences of $\eta_{oo,l}$, $\eta_{oo,a}$, and η_i between nWS- and WS-LD.

We analyzed slope efficiencies by fitting output power linearly to launched $P_{p,l}$ and absorbed $P_{p,a}$ pump power. The fitting results are presented in Figure 7, with the obtained parameters summarized in Table 2 and displayed in Figure 7e,f. As illustrated by a direct comparison in Figures 5b and 6c, the slope efficiencies $\eta_{sl,l}$ and $\eta_{sl,a}$ were consistently greater than their corresponding OO efficiencies $\eta_{oo,l}$ and $\eta_{oo,a}$. This phenomenon, widely observed in YDFLs [14,28,48], can be attributed to the negative y-intercepts of the linear fits depicted in Figure 7a,b.

These negative intercepts indicated the presence of an effective lasing threshold, defined by the intersection of the fitted line and the pump power axis. To compensate for the initial power offset, a steeper slope was required. Such effective thresholds are frequently connected with intrinsic cavity losses that must be overcome before lasing starts [36,49–51]. However, we identified a fundamentally different origin in our system. The effective threshold found here was not due to traditional cavity losses but rather to the pump's poor absorption efficiency at low power, which permitted a significant fraction of the pump light to escape without contributing to the gain.

In practice, differences in pump absorption efficiency at various launched power levels have a considerable impact on differential slope efficiency. The linear fits in Figure 7a,b reflect an average slope value that was dependent on the specific LD employed, thereby incorporating its distinct influence. Figure 7c,d show a more fundamental relationship between output power and absorbed pump power. Despite using two sets of LDs with significantly distinct emission spectra to pump the same oscillator, the resulting linear fits show intercepts that approached zero with a small error margin. The slope intervals

at 95% confidence levels were [0.6569, 0.6761] and [0.6629, 0.6883] for WS- and nWS-LD, respectively, indicating satisfactory convergence.

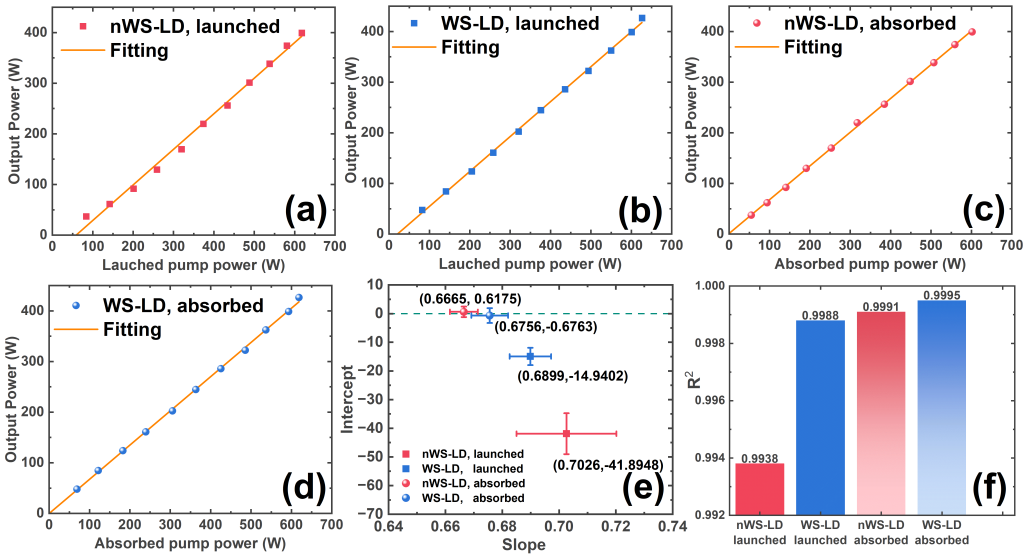

Figure 7. Fitting results of (**a**) nWS-LD at launched, (**b**) WS-LD at launched, (**c**) nWS-LD at absorbed, and (**d**) WS-LD at absorbed pump power. (**e**) Yielded slope and intercept with their errors. (**f**) Linear fitting goodness R^2.

Furthermore, the slope and OO efficiencies showed remarkable agreement across the full power range. This approach's validity was quantitatively verified by both the marked reduction in fitting parameter errors, shown in Figure 7e, and the greatly enhanced goodness-of-fit R^2, as illustrated in Figure 7f. The difference in slope efficiency between nWS- and WS-LDs originated from both η_p and measurement uncertainties when based on launched power, but primarily from the latter when based on absorbed power.

Table 2. Summary of linear fitting parameters yielded from fitting results in Figure 7.

Figure No.	Slope	Intercept	R^2	LD Type	Pump Power
(a)	0.7026 ± 0.0176	-41.8948 ± 7.1402	0.9938	nWS-LD	launched
(b)	0.6899 ± 0.0073	-14.9402 ± 3.0102	0.9988	WS-LD	launched
(c)	0.6756 ± 0.0065	-0.6763 ± 2.6029	0.9991	nWS-LD	absorbed
(d)	0.6665 ± 0.0049	0.6175 ± 1.8293	0.9995	WS-LD	absorbed

Variations in pump absorption efficiency produced equal changes in unabsorbed residual pump power. According to Equations (2) and (3), the magnitude of this residual power was determined by a complicated interplay between η_p and $P_{p,l}$. Figure 8a shows the calculated unabsorbed residual pump powers for WS- and nWS-LDs at various launched pump powers. This unabsorbed part of light was removed by the CPS and transformed into heat, causing an increase in temperature in the etched scattering region. A strong positive correlation was expected between residual pump power and temperature rise in both the CPS's etched region and housing. In our experiment, the observed rise in housing temperature was minimal, which could be attributed to the water-cooling method's excellent heat dissipation and relatively low absolute power levels. We used a CPS housing temperature coefficient of 0.066 °C/W of stripped power from Ref. [52]. The evolution of the housing temperature with launching power was computed using this coefficient and a linear assumption, as shown in Figure 8b, assuming an ambient temperature of 22 °C.

Figure 8 shows that the WS-LD consistently had lower residual pump power and CPS housing temperature than the nWS-LD due to its higher pump absorption efficiency across the full power range. Furthermore, both types of LD exhibited a non-monotonic evolution, with residual power increasing and then decreasing as pump power increased. The peak residual pump power and, thus, the greatest CPS housing temperature occurred at power that was neither the minimum pump absorption efficiency nor the maximum launched pump power, but rather at intermediate power.

For the WS-LD, this peak was at a pump power of 205 W, corresponding to 22.21 W of residual power and a housing temperature of 23.47 °C. In contrast, for the nWS-LD, the peak occurred at 259 W, with 67.79 W of residual power and a housing temperature of 26.47 °C. Experimentally, the real temperature of that could deviate from the theoretical value above due to potential sources, including the initial temperature of ambient and cooling water, the material of the CPS housing, and the convective coefficient of the related heat sink design.

These results clearly demonstrate the importance of pump absorption efficiency. As a result, our approach allows for a more precise calculation of the maximum residual pump power, surpassing naive estimations based purely on the quantum defect, which would result in significant underestimation and a serious thermal management risk in high-power YDFLs. These findings provide a critical refinement to the design of thermal management systems in complicated YDFL architectures.

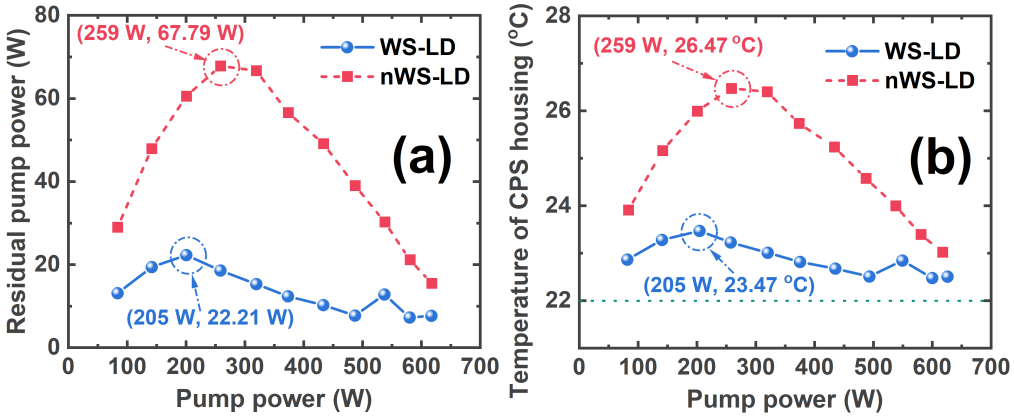

Figure 8. (**a**) Residual pump power and (**b**) temperature of CPS housing versus pump power for WS- and nWS-LD.

5. Conclusions

In summary, we systematically investigated and quantified the profound impact of LD spectral characteristics on the overall efficiency of YDFLs. Our approach began by deconstructing the conventional OO efficiency into three fundamental components: the pump absorption efficiency, the quantum conversion efficiency, and the intrinsic laser efficiency. This framework clarified the distinct relationship between efficiencies calculated from launched versus absorbed pump power.

We built a YDFL oscillator and subjected it to pumping by two different LD groups, one with WS spectra and the other with nWS. Through meticulous characterization of both the pump spectra and the resulting laser performance, we showed that the widely observed inconsistencies in OO and slope efficiencies were primarily governed by variations in pump absorption efficiency, with the influence of the quantum defect being negligible. By referencing the output power to the absorbed pump power, we effectively separated the system's inherent performance from the LD's spectral properties, demonstrating consistent and predictable OO and slope efficiencies regardless of pump source configuration. Fur-

thermore, our research reveals a non-monotonic growth of the unabsorbed residual pump power, indicating that the peak thermal load on the CPS does not always correspond to the highest launched pump power but rather occurs at an intermediate power level. This crucial finding challenges conventional thermal management design, which frequently relies only on quantum defect estimates. Such an approach can lead to a significant underestimation of peak thermal load, thereby posing a substantial risk to the long-term operational reliability of high-power YDFL systems.

The approach and insights presented in this work not only establish a more precise technique of characterizing and predicting YDFL performance but also serve as an important guideline for the design of LDs with tailored spectral profiles. This allows for the accurate engineering of pump absorption, resulting in an optimal balance of nonlinear effect suppression and TMI mitigation. Finally, this illustrates diverse strategies for adapting the performance of particular laser designs to specific application requirements.

Author Contributions: Conceptualization, F.L., Y.S., L.H., and C.Z.; methodology, R.T., Q.C., and H.Z.; validation, Y.S. and Q.S.; formal analysis, F.L., Y.S., and C.Z.; investigation, Y.W., X.J., and Z.G.; resources, H.Z. and H.L.; data curation, Y.S.; writing—original draft preparation, F.L. and Y.S.; writing—review and editing, R.T.; visualization, F.L.; supervision, H.L.; project administration, H.L. All authors have read and agreed to the published version of the manuscript.

Funding: This work was supported by the National Natural Science Foundation of China (no. 62205317).

Institutional Review Board Statement: Not applicable.

Informed Consent Statement: Not applicable.

Data Availability Statement: Data is contained within the article.

Conflicts of Interest: The authors declare no conflicts of interest.

References

1. Horley, R.; Norman, S.; Zervas, M.N. Progress and development in fibre laser technology. *Proc. SPIE* **2007**, *6738*, 67380K. [CrossRef]
2. Nilsson, J.; Payne, D.N. High-power fiber lasers. *Science* **2011**, *332*, 921–922. [CrossRef]
3. Jauregui, C.; Limpert, J.; Tünnermann, A. High-power fiber lasers. *Nat. Photon.* **2013**, *7*, 861–867. [CrossRef]
4. Zervas, M.N.; Codemard, C.A. High power fiber lasers: A Review. *IEEE J. Sel. Top. Quantum Electron.* **2014**, *20*, 219–241. [CrossRef]
5. Li, X.; Yu, H.; Zou, S.; He, C.; Ning, C.; Wu, W.; Chen, X.; Lin, X. A 606 W burst-mode picosecond Yb-doped all-fiber laser with an intra-burst repetition rate of 469 MHz. *High Power Laser Sci. Eng.* **2024**, *12*, e87. [CrossRef]
6. Yang, S.; Smith, C.R.; Petersen, C.R.; Bang, O. All-Fiber 2 μm Mamyshev Oscillator: Mapping of Different Operating Regimes. *Laser Photon. Rev.* **2025**, *19*, 2500074. [CrossRef]
7. Li Y.; Zhong Z.; Zhang L.; Wei Z.; Khalil, D.; Kotb, H.; Wei, H.; Zhu, M.; Wen, J.; Pang, F.; et al. Replica symmetry breaking dynamics in high-order optical mode multi-Stokes coherent random fiber laser. *APL Photon.* **2025**, *10*, 070804. [CrossRef]
8. Ermolaev, M.; Moshegov, N.; Berezin, I.; Trubenko, P.; Shifrovich, I.; Berishev, I.; Mukhametzhanov, I.; Chuyanov, V.; Kompan, F.; Miftakhutdinov, D.; et al. Next-generation high-power laser diode pump modules. *Proc. SPIE* **2025**, *13345*, 133450D. [CrossRef]
9. Ding, L.; Liu, P.; Chen, H.; Huang, L. Advance on the high-power and high-brightness diode laser modules for pumping and direct use applications. *Proc. SPIE* **2024**, *12867*, 128670V. [CrossRef]
10. Wu, J.; Wan, Y.; Wang, P.; Zhang, H.; Wang, X.; Zhou, P.; Du, S.; Xu, X. Wide temperature operation of kilowatt fiber oscillators. *Appl. Opt.* **2022**, *61*, 417–421. [CrossRef]
11. Paschotta, R.; Nilsson, J.; Tropper, A.; Hanna, D. Ytterbium-doped fiber amplifiers. *IEEE J. Quantum Electron.* **1997**, *33*, 1049–1056. [CrossRef]
12. Liu, X.; Hu, M.; Caneau, C.; Bhat, R.; Zah, C. Thermal management strategies for high power semiconductor pump lasers. *IEEE Trans. Compon. Packag. Technol.* **2006**, *29*, 268–276. [CrossRef]
13. Hejaz, K.; Norouzey, A.; Poozesh, R.; Heidariazar, A.; Roohforouz, A.; Nasirabad, R.R.; Jafari, N.T.; Golshan, A.H.; Babazadeh, A.; Lafouti, M. Controlling mode instability in a 500 W ytterbium-doped fiber laser. *Laser Phys.* **2014**, *24*, 025102. [CrossRef]
14. Yang, M.; Wang, P.; Xu, X.; Wu, H.; Pan, Z.; Ye, Y.; Yan, Z.; Xi, X.; Zhang, H.; Wang, X. 1010 nm directly LD-pumped 6kW monolithic fiber laser employing long-tapered Yb^{3+}-doped fiber. *Photonics* **2024**, *11*, 1033. [CrossRef]

15. Chen, J.; Wu, J.; Li, F.; Peng, W.; Wu, H.; Zhang, H.; Wang, X. Kilowatt high power ytterbium-doped fiber laser operation in a record wide temperature range from −50 °C to 50 °C. *Opt. Express* **2024**, *32*, 47098–47110. [CrossRef]
16. Li, Q.; Zhang, H.; Shen, X.; Yan, P.; Hao, H.; Gong, M. Stimulated Raman scattering threshold for partially coherent light in silica fibers. *Opt. Express* **2024**, *23*, 28438–28448. [CrossRef]
17. Zeng, L.; Wang, X.; Wang, L.; Ye, Y.; Wang, P.; Yang, B.; Xi, X.; Pan, Z.; Zhang, H.; Shi, C.; et al. Optimization and demonstration of direct LD pumped High-Power fiber lasers to balance SRS and TMI effects. *Photonics* **2023**, *10*, 539. [CrossRef]
18. Tian, X.; Rao, B.; Wang, M.; Xi, X.; Yang, B.; Chen, Z.; Xiao, H.; Wang, X.; Ma, P.; Wang, Z.; et al. 6 kW single stage narrow linewidth fiber amplifier based on the balance between mode instability and nonlinear effects. *IEEE Photon. J.* **2023**, *15*, 1502105. [CrossRef]
19. Dawson, J.W.; Messerly, M.J.; Beach, R.J.; Shverdin, M.Y.; Stappaerts, E.A.; Sridharan, A.K.; Pax, P.H.; Heebner, J.E.; Siders, C.W.; Barty, C. Analysis of the scalability of diffraction-limited fiber lasers and amplifiers to high average power. *Opt. Express* **2008**, *16*, 13240. [CrossRef]
20. Tao, R.; Ma, P.; Wang, X.; Zhou, P.; Liu, Z. Mitigating of modal instabilities in linearly-polarized fiber amplifiers by shifting pump wavelength. *J. Optics.* **2015**, *17*, 4–7. [CrossRef]
21. Tao, R.; Ma, P.; Wang, X.; Zhou, P.; Liu, Z. Study of wavelength dependence of mode instability based on a semi-analytical model. *IEEE J. Quantum Electron.* **2015**, *51*, 1600106. [CrossRef]
22. Wan, Y.; Yang, B.; Wang, P.; Xi, X.; Zhang, H.; Wang, X. Optimizing the pump wavelength to improve the transverse mode instability threshold of fiber laser by 3.45 times. *J. Modern Opt.* **2021**, *68*, 967–974. [CrossRef]
23. Wan, Y.; Yang, B.; Xi, X.; Zhang, H.; Wang, P.; Wang, X.; Xu, X. Comparison and optimization on transverse mode instability of fiber laser amplifier pumped by wavelength-stabilized and non-wavelength-stabilized 976 nm laser diode. *IEEE Photon. J.* **2022**, *14*, 1503905. [CrossRef]
24. Rezaei-Nasirabad, R.; Azizi, S.; Paygan, D.; Tavassoli, M.; Abedinajafi, A.; Roohforouz, A.; Chenar, R.E.; Golshan, A.H.; Hejaz, K.; Vatani, V. 2.5 kW TMI-free co-pump Yb-doped fiber oscillator by 971.5 nm pumping wavelength. *Opt. Laser Technol.* **2023**, *157*, 108652. [CrossRef]
25. Wan, Y.; Xi, X.; Shen, Y.; Wang, X. Influence of central wavelength of pump source and pump direction on transverse mode instability threshold of fiber laser. *Opt. Laser Technol.* **2023**, *162*, 109270. [CrossRef]
26. Huang, Z.; Tang, X.; Zhao, P.; Li, Z.; Li, C.; Li, Q.; Guo, C.; Lin, H.; Wang, J.; Jing, F. Influence of spectral properties of wavelength-locked and wavelength-unlocked diode laser on fiber laser performances. *Laser Phys.* **2016**, *26*, 075104. [CrossRef]
27. Meng, X.; Li, F.; Yang, B.; Wang, P.; Yan, Z.; Yan, Z.; Ye, Y.; Xi, X.; Zhang, H.; Pan, Z.; et al. A 5 kW nearly-single-mode monolithic fiber laser emitting at ~1050 nm employing asymmetric bi-tapered ytterbium-doped fiber. *Photonics* **2023**, *10*, 1158. [CrossRef]
28. Meng, X.; Li, F.; Yang, B.; Ye, Y.; Chai, J.; Xi, X.; Wang, P.; Wu, H.; Shi, C.; Zhang, H.; et al. A 4.8-kW high-efficiency 1050-nm monolithic fiber laser amplifier employing a pump-sharing structure. *Front. Phys.* **2023**, *11*, 1255125. [CrossRef]
29. Meng, X.; Li, F.; Chen, J.; Xi, X.; Yang, B.; Wang, P.; Pan, Z.; Yan, Z.; Zhang, H.; Wang, X.; et al. 20 kW monolithic fiber amplifier with directly dual-wavelength laser diodes counter pumping. *IEEE Photon. J.* **2024**, *16*, 1503006. [CrossRef]
30. Zeng, L.; Wen, Y.; Wang, X.; Wang, P.; Xi, X.; Yang, B.; Zhang, H.; Xi, F.; Han, K.; Wang, Z.; et al. Experimental research on abnormal transverse mode instability in high-power fiber lasers. *Chin. J. Lasers* **2024**, *51*, 0601001. [CrossRef]
31. Tao, R.; Wang, X.; Zhou, P. Comprehensive Theoretical Study of mode instability in High-Power Fiber Lasers by employing a universal Model and its implications. *IEEE J. Sel. Top. Quantum Electron.* **2018**, *24*, 0903319. [CrossRef]
32. Jauregui, C.; Stihler, C.; Limpert, J. Transverse mode instability. *Adv. Opt. Photon.* **2020**, *12*, 429. [CrossRef]
33. Dong, L.; Ballato, J.; Kolis, J. Power scaling limits of diffraction-limited fiber amplifiers considering transverse mode instability. *Opt. Express* **2023**, *31*, 6690. [CrossRef]
34. Abakumov, G.; Vorob'ev, S.; Simonov, A. Induced pump absorption, lasing threshold, and efficiency of organic compound lasers. *Sov. J. Quantum Electron.* **1977**, *7*, 1094. [CrossRef]
35. Petričević, V.; Seas, A.; Alfano, R. Slope efficiency measurements of a chromium-doped forsterite laser. *Opt. Lett.* **1991**, *16*, 811. [CrossRef]
36. Laporta, P.; Brussard, M. Design criteria for mode size optimization in diode-pumped solid-state lasers. *IEEE J. Quantum Electron.* **1991**, *27*, 2319. [CrossRef]
37. Wagener, J.; Wysocki, P.; Digonnet, M.F.; Shaw, H. Effect of concentration on the efficiency of erbium-doped silica fiber lasers. *Proc. SPIE* **1993**, *1789*, 80. [CrossRef]
38. Dimov, S. Dynamical behaviour and harmonic generation of a 946-nm pulsed, flashlamp-pumped Nd:YAG laser. *Opt. Quantum Electron.* **1993**, *25*, 545. [CrossRef]
39. Sun, J.; Liu, L.; Han, L.; Zhu, Q.; Shen, X.; Yang, K. 100 kW ultra high power fiber laser. *Opt. Contin.* **2022**, *1*, 1932. [CrossRef]
40. Zervas, M.N.; Marshall, A.; Kim, J. Effective absorption in cladding-pumped fibers. *Proc. SPIE* **2011**, *7914*, 79141T. [CrossRef]
41. Jacquier, B. *Rare Earth-Doped Fiber Lasers and Amplifiers*; Springer: Boston, MA, USA, 1997. [CrossRef]

42. Becker, P.C.; Olsson, N.A.; Simpson J.R. *Erbium-Doped Fiber Amplifiers: Fundamentals and Technology*; Academic Press: Cambridge, MA, USA, 1999. [CrossRef]
43. Koester, C.J.; Snitzer, E. Amplification in a fiber laser. *Appl. Opt.* **1964**, *3*, 1182–1186. [CrossRef]
44. Li, D.; Wang, T.; Zhao, J.; Rao, L. Influence of ambient temperature on the performance of the semiconductor laser. In Proceedings of the 15th International Conference on Optical Communications and Networks (ICOCN), Hangzhou, China, 24–27 September 2016. [CrossRef]
45. Redlich, C.; Lingnau, B.; Huang, H.; Raghunathan, R.; Schires, K.; Poole, P.; Grillot, F.; Ludge, K. Linewidth rebroadening in quantum dot semiconductor lasers. *IEEE J. Sel. Top. Quantum Electron.* **2017**, *23*, 1901110. [CrossRef]
46. Andreou, S.; Williams, K.A.; Bente, E.A.J.M. Monolithically integrated InP-based DBR lasers with an intra-cavity ring resonator. *Opt. Express* **2019**, *27*, 26281. [CrossRef]
47. Agrawa, G.P. *Nonlinear Fiber Optics*, 5th ed.; Academic Press: Cambridge, MA, USA, 2013. [CrossRef]
48. Ye, Y.; Meng, X.; Xi, X.; Yan, Z.; Yang, B.; Pan, Z.; Wu, H.; Zhang, H.; Shi, C.; Wang, X.; et al. Towards a tapered Yb-doped fiber-based narrow linewidth single-mode fiber laser with a high signal to Raman ratio. *Opt. Express* **2023**, *31*, 26831. [CrossRef] [PubMed]
49. Fu, C.; Li, Y.; Liu, W.; Lu, F.; Lu, K. Conversion efficiency of double-clad fiber laser. *SPIE* **2000**, *4225*, 160–163. [CrossRef]
50. Caird, J.; Payne, S.; Staber, P.; Ramponi, A.; Chase, L.; Krupke, W. Quantum electronic properties of the $Na_3Ga_2Li_3F_12:Cr^{3+}$ laser. *IEEE J. Quantum Electron.* **1988**, *24*, 1077. [CrossRef]
51. Ramírez, M.; Jaque, D.; García, J.S.; Bausá, L.; Santiuste, J.M. 74% Slope efficiency from a diode-pumped Yb^{3+}:$LiNbO_3$:MgO laser crystal. *Appl. Phys. B* **2003**, *77*, 621–623. [CrossRef]
52. Liu, Y.; Li, M.; Huang, S.; Wu, W.; Feng, X.; Shen, B.; Song, H.; Tao, R.; Wang, J.; Jing, F. >500 W passively-cooled fiber cladding light stripper. *High Power Laser Part Beams* **2021**, *33*, 021005. [CrossRef]